Hydrology and Earth System Sciences, 3(3), *375–384* (1999) © EGS

Hydrology & Earth System Sciences

Groundwater-surface water interaction and the climatic spatial patterns of hillslope hydrological response

Cornelis P. Kim,[1] Guido D. Salvucci[2] and Dara Entekhabi*[3]

[1] Boston Consulting Group, Baarn, The Netherlands
[2] Departments of Earth Sciences and Geography, Boston University, Boston, Massachusetts 02215 U.S.A.
[3] 48-331 Ralph M. Parsons Laboratory, Massachusetts Institute of Technology, Cambridge, Massachusetts 02139 U.S.A.
* e-mail address for corresponding author: darae@mit.edu

Abstract

A transient, mixed analytical-numerical model of hillslope hydrological behaviour is used to study the patterns of infiltration, evapotranspiration, recharge and lateral flow across hillslopes. Computational efficiency is achieved by treating infiltration and phreatic surface movement analytically. The influence of dynamic coupling of the saturated and unsaturated zones on the division of hillslopes into units of distinct hydrological behaviour is analyzed. The results indicate the importance of downhill groundwater flow on the lateral distribution of soil moisture and hydrological fluxes; unsaturated lateral flow is shown to be of relatively minor importance. For most conditions, the hillslope organizes itself into three distinct regions; an uphill recharge and a downhill discharge zone separated by a midline zone over which there is, on average, no recharge or discharge. A temporal perturbation analysis of the phreatic surface, made to quantify the deviations between the equivalent-steady water table derived by Salvucci and Entekhabi (1995) and the long-term mean water table, shows that the equivalent-steady water table effectively couples the unsaturated and saturated zone dynamics across storm and interstorm periods and divides the hillslope into distinct hydrological regions. The second order closure terms in the perturbation analysis, expressed as the gradient of water table variance, quantify the deviations and tend to make the hydrological zones relatively less distinct.

Introduction

Spatial heterogeneity of the soil water states and fluxes along the land surface may be caused by: 1) spatial variation of the soil and vegetation characteristics, 2) spatial variation of the atmospheric boundary conditions such as precipitation and potential evapotranspiration and 3) lateral topographic redistribution of water. Peck *et al.* (1977), Milly and Eagleson (1987), Kim and Stricker (1996), and others studied the impact of the first two sources of heterogeneity on the areally averaged water budget using Monte Carlo simulations. Beven and Kirkby (1979), Sivapalan *et al.* (1987), Salvucci and Entekhabi (1995), Dawes *et al.* (1997) and many others have studied the mechanisms through which lateral redistribution along hillslopes affects the partitioning of rainfall into surface runoff, evapotranspiration and groundwater runoff. In contrast to the statistical nature of soil and vegetation heterogeneity, lateral redistribution is due to topographic controls and contributes to the spatial variability of hydrological fluxes in a structured manner. Such deterministic contribution to the total heterogeneity of soil moisture and hydrological fluxes has significant implications for the upscaling and aggregation of hydrological processes.

Freeze and Witherspoon (1968) recognized that the shape of the phreatic surface and the conditions in the unsaturated zone are mutually dependent. Infiltration and evapotranspiration are related to the water table depth, and the recharge of the groundwater depends on the partitioning of rainfall over infiltration and surface runoff and, in return, of infiltration over evapotranspiration and deep percolation.

Salvucci and Entekhabi (1995) analyzed the impact of this mutual interdependence on the spatial structure of hillslope hydrological processes by extending to two dimensions the statistical-dynamical point water balance model of Eagleson (1978a). They solve the groundwater flow system on rectangular sloping domains subject to the long-term average percolation from and capillary rise to the unsaturated zone. The unsaturated zone model in Salvucci and Entekhabi (1995) expresses these mean vertical hydrological fluxes as a function of soil and climate parameters as well as of the long-term position of the water table. The resulting equivalent-steady state system solved

by Salvucci and Entekhabi (1995) indicates the importance of groundwater-surfacewater interaction in determining the spatial structure of hydrological fluxes. For example, downhill riparian zones that evaporate at the potential rate much longer than uphill areas arise because of downslope lateral groundwater flow that occurs under a midline region of zero mean recharge, similar to the field observations of Toth (1966). This study considers a similar problem as Salvucci and Entekhabi (1995), except that here there will be constructed and deployed a fully transient saturated/unsaturated model of hillslope hydrological behaviour. With this model the role of transients and lateral unsaturated flow on the organization of recharge and discharge zones will be examined. Furthermore the deviations between the equivalent-steady and temporal-mean water table will be quantified.

While inclusive models of coupled saturated/unsaturated water flow exist in the literature (e.g. Freeze, 1971; Paniconi and Wood, 1993), a mixed analytical-numerical model is presented here. In this hybrid approach, the computationally most intensive processes at the boundaries of the domain (infiltration and movement of the phreatic surface) are treated analytically. In a similar approach, Smith and Hebbert (1983) used kinematic wave theory to describe downward unsaturated flow in response to storm events. However, since kinematic waves travel in one direction only, their model does not account for upward capillary flow from the ground water which may be induced by interstorm evaporation periods.

Below, the unsaturated and saturated flow equations that constitute the backbone of the model are presented as well as the initial and boundary conditions. The numerical methods and the analytical treatment of the processes that are computationally most demanding are outlined afterwards. For a simple geometry hillslope, the model is used to examine the dynamics of saturated and unsaturated zones and to study the development of hydrological regions with distinguishing characteristics.

Flow equations and their numerical implementation

FLOW EQUATIONS

The simple hillslope (with slope angle ϕ) shown in Fig. 1 consists of an unsaturated and a saturated domain, separated by the phreatic surface. The soil surface and the impermeable layer are the upper and lower boundaries of the unsaturated and saturated zones respectively. The coordinate system has an x-direction parallel to the impermeable layer and a z-direction normal to it. The origin is taken at the most downhill location of the impermeable layer. The soil depth is indicated by z_s and may vary with x. In the model, fluxes towards the origin are taken as being positive, as illustrated in Fig. 1.

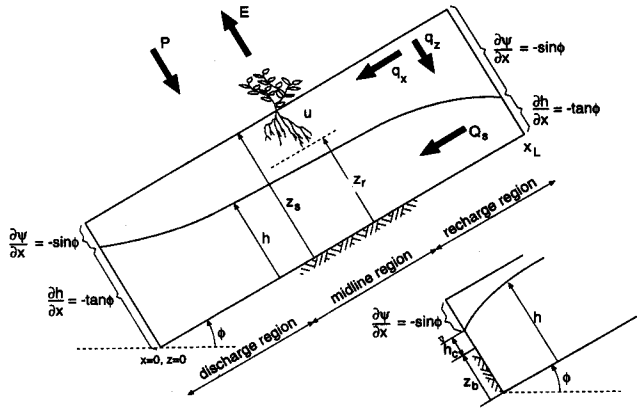

Fig. 1. *Schematic overview of the hillslope model domain and boundary conditions. The inset shows the lower boundary in case of a channel. The symbols are outlined in the text.*

UNSATURATED DOMAIN

The Darcy fluxes in the x and z direction for an isotropic unsaturated medium take the form

$$q_x = k(\theta)\left(\frac{\partial\psi}{\partial x} + \sin\phi\right) \tag{1}$$

$$q_z = k(\theta)\left(\frac{\partial\psi}{\partial z} + \cos\phi\right) \tag{2}$$

where k is the hydraulic conductivity, θ is the volumetric moisture content and ψ is the soil matric head. Anisotropy may be accounted for by distinguishing between k_x and k_z. Combination of (1) and (2) with the mass conservation equation yields the two dimensional Richards equation which, after addition of a sink term U for water uptake by plant roots, is written as

$$\frac{\partial\theta(\psi)}{\partial t} = -\left(\frac{\partial}{\partial x}\left[k(\theta)\left(\frac{\partial\psi}{\partial x} + \sin\phi\right)\right] + \frac{\partial}{\partial z}\left[k(\theta)\left(\frac{\partial\psi}{\partial z} + \cos\phi\right)\right] + U(\theta)\right) \tag{3}$$

The soil hydraulic characteristics $\theta(\psi)$ and $k(\theta)$ are described according to Van Genuchten (1980):

$$\theta(\psi) = s(\psi)(\theta_s - \theta_r) + \theta_r \tag{4}$$

$$s(\psi) = \left(1 + |a_g\psi|^{n_1}\right)^{-n_2} \tag{5}$$

$$k(\theta) = k_s s^l\left[1 - \left(1 - s^{\frac{1}{n_2}}\right)^{n_2}\right]^2 \tag{6}$$

where s is the saturation degree, a_g, l, n_1, are parameters, k_s is the saturated conductivity, and $n_2 = 1 - (1/n_1)$.

Water uptake in the root zone of depth $z_s - z_r$ is mod-

elled as a function of potential evaporation (E_p) and moisture content as:

$$U(\theta) = \begin{cases} \beta(\theta)\frac{E_p}{z_s - z_r} & z_r \le z \le z_s \\ 0 & 0 \le z \le z_r \end{cases} \quad (7)$$

where

$$\beta(\theta) = \begin{cases} 1 & \theta_c < \theta \le \theta_s \\ \frac{\theta - \theta_w}{\theta_c - \theta_w} & \theta_w \le \theta \le \theta_c \\ 0 & 0 \le \theta < \theta_w \end{cases} \quad (8)$$

with θ_c and θ_w the critical and wilting point moisture contents respectively (Feddes, 1978). Because the principal state variable of the model is the volumetric moisture content, transpiration efficiency is expressed in terms of θ rather than ψ. The root density is assumed to be uniform over the depth of the root zone, but other distributions may be easily implemented. The total evapotranspiration is obtained through integration of the water uptake U over the depth of the rootzone.

SATURATED DOMAIN

When neglecting saturated flow in the z-direction (Dupuit assumption), one-dimensional saturated lateral flow in the x-direction, Q_s, is given by the Boussinesq equation

$$Q_s = k_s h \cos\phi \left(\frac{\partial h}{\partial x} + \tan\phi \right) \quad (9)$$

where h is the height of the phreatic surface above the impermeable layer as depicted in Fig. 1. Irregularities of the impermeable layer can be taken into account easily by replacing h in Eqn. (9) with $h - z_b$, where z_b indicates a local deviation from the $z = 0$ level.

Applying the continuity principle, the time rate of change of the phreatic surface is given by

$$S_y(x,t)\frac{\partial h}{\partial t} = q_r - \frac{\partial}{\partial x}\left(k_s h \cos\phi \left[\frac{\partial h}{\partial x} + \tan\phi \right] \right) \quad (10)$$

where S_y stands for the specific yield, i.e. the empty pore space available to water storage above the water table. In the forthcoming section on the analytical treatment of the phreatic surface, a solution to the problem of specifying values for S_y is presented. Recharge q_r is given by the one-dimensional Darcy flux that is dependent on the soil moisture profile:

$$q_r = k_z(\psi)\left(\frac{\partial \psi}{\partial z} + \cos\phi \right)\Big|_{z=h} \quad (11)$$

From these governing equations, the saturated and unsaturated zones are coupled through the recharge flux (11) and continuity of the pressure profile (i.e. $\psi = h$ at the water table). Since the strongest flow-inducing gradients are vertical in the unsaturated zone, lateral variations in hydrological conditions are governed mainly by saturated lateral flow (9) and the coupling in (11). Therefore, realistic treatment of the spatial heterogeneity of hydrological response in sloping areas requires the consideration of the entire coupled saturated-unsaturated system represented by the governing equations (1) through (11).

INITIAL AND BOUNDARY CONDITIONS

To solve the above equations, initial and boundary conditions need to be specified. Unless the initial conditions are known exactly, they are chosen arbitrarily and the model is allowed to spin-up to ensure that their effect is diminished.

In the case of a rainfall event, the upper boundary condition for the unsaturated domain switches from flux to head controlled infiltration whenever the soil surface is saturated and is no longer capable of absorbing all the rain falling on it. From that time onwards, a water layer develops at the surface, running downhill (infiltration excess runoff q_{ie}). If the phreatic surface reaches the ground surface, it acts as an impervious layer and all rain falling on it is removed as saturation excess overland flow q_{se}. Mathematically, the infiltration rate i is given by

$$i(x,t) = \begin{cases} P(t) & \psi(x,z_s,t) < 0 \\ k_s\left(\frac{\partial \psi}{\partial z} + \cos\phi \right)\Big|_{z=z_s} & \psi(x,z_s,t) = 0 \\ 0 & h(x,t) = z_s(x) \end{cases} \quad (12)$$

Note that (12) neglects the small positive pressure due to ponding at the surface. To resolve the infiltration process using a numerical solution of (12), high resolutions in space and time would be necessary (of the order of millimeters and seconds respectively). An analytical treatment of infiltration has, therefore, been adopted which will be discussed later.

The lower boundary condition for the unsaturated flow domain, which makes up the upper boundary condition for the saturated domain, is the atmospheric pressure at the phreatic surface

$$\psi = 0 \qquad z = h(x) \quad (13)$$

The last two boundary conditions for the unsaturated flow domain are the no-flow conditions at the vertical uphill (divide) and downhill (valley) boundaries

$$\frac{\partial \psi}{\partial x} = -\sin\phi \quad \begin{cases} h(0) < z \le z_s(0) \\ h(x_L) < z < z_s(x_L) \end{cases} \quad (14)$$

As for the unsaturated zone, no saturated flow is allowed at the divide and, because of hillslope symmetry, in the valley:

$$\frac{\partial h}{\partial x} = -\tan\phi \qquad x = 0, \quad x = x_L \quad (15)$$

When, at the downhill boundary, a channel with an elevation z_b is present in which a water level h_c is maintained (see inset Fig. 1), (15) is replaced by

$$h = z_b + h_c \quad x = 0 \tag{16}$$

A seepage face is adjacent to the downhill boundary when the groundwater reaches the soil surface. The uphill boundary of the seepage face depends on the transient flow conditions:

$$h = z_s(x) \qquad 0 < x \leq x_{sf}(t) \tag{17}$$

where x_{sf} is the most uphill position where the seepage face is present. The numerical treatment of the seepage face is discussed later.

Model formulation

The objective of the model requires two conflicting conditions to be satisfied. Accurate numerical solution of the system of transient nonlinear equations can only be achieved by using a high resolution in both space and time. A high resolution discretization, however, is computationally intensive and would prohibit long time integrations of the model. To compromise both requirements, the computationally most demanding processes, transient infiltration (12) and movement of the phreatic surface (10) are treated analytically while the other processes within the computational domain are solved numerically over a discrete grid.

NUMERICAL IMPLEMENTATION

The equations (1), (2) and (9) are approximated using their finite difference form. Interblock conductivities for the unsaturated fluxes are taken as the geometric mean of the neighbouring cells and, for the saturated fluxes, the arithmetic mean is used. Zaidel and Russo (1993) present a more accurate estimation of the unsaturated interblock conductivities which improves the accuracy of numerical solutions, especially for infiltration into dry soils. In the present model, however, the infiltration is treated analytically, thereby reducing the possible improvements of using more advanced weighing schemes. Solution of (3) uses an explicit finite difference scheme in time, whereas (10) is treated analytically, as will be explained shortly.

ANALYTICAL FORMULATION OF INFILTRATION

The method used to estimate infiltration fluxes accounts for intervals of low rain rates, during which a ponded surface unponds temporarily and soil moisture redistributes. In the following, the treatment of switching from unponded to ponded infiltration is outlined.

As indicated in (12), when the phreatic surface reaches the surface ($h = z_s$) all rainfall is removed as saturation excess runoff q_{se}. Otherwise, given a vertically uniform moisture content θ_i at the beginning of a rainfall event t_i the method predicts the ponding time t_p at which the boundary condition (12) switches from flux controlled to head controlled. Mathematically, the infiltration flux is

$$i(t) = \begin{cases} \min\{P(t), i_h(t)\} & h < z_s \\ 0 & h = z_s \end{cases} \tag{18}$$

where the head controlled infiltration i_h rate, corrected for the slope angle, is given by Smith *et al.* (1993) as

$$i_h(t) = k_s\left(\cos\phi + \left[\exp\left(\frac{2[i^{cum}(t) - k(\theta_i)t]k_s}{S^2(\theta_i)}\right) - 1\right]^{-1}\right) \tag{19}$$

in which

$$S^2(\theta_i) \cong 2(\theta_s - \theta_i)\int_{\theta_i}^{\theta_s} D(\theta)d\theta \tag{20}$$

where

$D(\theta) = k(\theta)(d\psi/d\theta)$ S is sorptivity and $i^{cum}(t)$ denotes the cumulative infiltration since the beginning of the storm event (Kutilek and Nielsen, 1994). Except for very high initial moisture contents, $k(\theta_i)t \ll i^{cum}$ and is neglected.

In (18) infiltration $i^{cum}(t)$ accumulates from any pattern $P(t)$ ($P > k_s$) until the rainfall rate encounters the curve $i_h(t)$ (at $t = t_p$), after which i^{cum} accumulates from $i_h(t)$. This behaviour is based on the time compression approximation (TCA). TCA essentially uses cumulative infiltration as a surrogate for time, which is explicit in (19).

Due to the transient nature of the model, the condition of a uniform initial profile is generally not met. Water uptake by roots, however, tends to homogenize the moisture profile in the root zone, thereby relaxing the severity of the assumption. Roots are sinks farther away from the surface boundary sink (surface evaporation). With roots, the soil moisture profile tends to become more uniform with depth rather than decreasing monotonically towards the surface. In the model, sorptivity S is determined using the soil moisture status of the grid cell closest to the soil surface.

ANALYTICAL TREATMENT OF THE PHREATIC SURFACE DYNAMICS

The height of the groundwater table determines to a great extent the lateral water fluxes as well as the moisture profile and vertical fluxes in the unsaturated zone above it. Hence, the location of the phreatic surface needs to be determined with considerable accuracy. To keep track of the phreatic surface while using a coarse vertical discretization, a simple analytical treatment has been adopted that allows for subgrid movement. The method described below replaces the numerical solution of (10) at the water

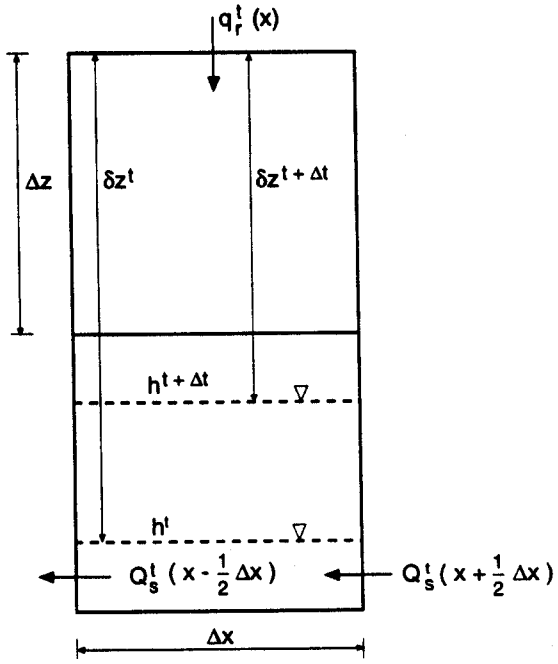

Fig. 2. *Diagram explaining the updating of the phreatic surface going from t to t + Δt. The height of the hydrostatic region is indicated δz.*

table interface, thus replacing the need to define the (problematic) specific yield (S_y).

Consider the vertical cross-section in Fig. 2. A region above the phreatic surface of height δz is assumed to be in hydrostatic equilibrium with the groundwater table, i.e. $\psi = h - z$. Any flux going into or out of this relatively very moist region is assumed to equilibrate instantaneously with the phreatic surface, because the hydraulic conductivity is high. The height of the hydrostatic region ($\Delta z < \delta z < 2\Delta z$) at any location x and time $t+\Delta t$ can be solved implicitly by formulating the mass balance at time t for the two grid cells containing the phreatic surface and the hydrostatic zone:

$$(2\Delta z - \delta z^{t+\Delta t})\theta_s + \int_{-\delta z^{t+\Delta t}}^{0} \theta(\psi)d\psi = (2\Delta z - \delta z^t)\theta_s + \int_{-\delta z^t}^{0} \theta(\psi)d\psi + \left(\frac{Q_s^t\left(x+\frac{1}{2}\Delta x\right) - Q_s^t\left(x-\frac{1}{2}\Delta x\right)}{\Delta x}\right)\Delta t + q_r^t \Delta t \tag{21}$$

The left-hand-side terms of (21) represent the total water stored in the two grid cells at time $t + \Delta t$. The right-hand-side terms represent the sum of the storage at time t, the time-step net lateral flux to the grid cell, and the time-step recharge from above. As indicated in Fig. 2, the recharge flux q_r^t is determined via (2) at the top of the hydrostatic zone rather than right at the phreatic surface as suggested by (11).

In case the hydrostatic zone moves into another grid cell, $\delta z^{t+\Delta t}$ can be determined implicitly by formulating the mass balance for three grid cells. Since no analytical integration of $\theta(\psi)$ in (4) is possible, $\theta(\psi)$ is assumed to be linear for the short distance $-\delta z \,''\, \psi \,''\, 0$:

$$\int_{-\delta z}^{0} \theta(\psi)d\psi \approx \frac{\theta_s + \theta(-\delta z)}{2}\delta z \tag{22}$$

This assumption introduces little error as long as δz is smaller than the height of the capillary fringe, the zone above the water table that is close to saturation. Because $\delta z < 2\,\Delta z$, the error in the above linearization is thus small when the vertical grid distance z is chosen to be smaller than half the height of the capillary fringe. Troch *et al.* (1993) in their Eqn. (18) provide a closed mathematical formulation that may be used in place of this approximate approach.

The rise of the phreatic surface is determined by the length of the time step Δt. To prevent large changes of the phreatic surface, the length of a time step is restricted. For the time steps used for the computations in this paper (< 10 min), the movement of the phreatic surface is small in comparison to the height of a grid cell.

When the phreatic surface comes close to the soil surface ($h > z_s - 2\Delta z$), the hydrostatic zone is assumed to extend up to the soil surface. The limited empty pore space available for water storage then causes the phreatic surface to react in a very pronounced way to small amounts of water that are either extracted or supplied. When the phreatic surface reaches the soil surface, a seepage face develops.

TREATMENT OF THE SEEPAGE FACE

In the absence of rain, flow out of the seepage face is described as the divergence of the lateral saturated flow minus the actual evapotranspiration over the seepage face:

$$q_{sf}(x) = \frac{Q_s(x+\frac{1}{2}\Delta x) - Q_s(x-\frac{1}{2}\Delta x)}{\Delta x} - E(x) \tag{23}$$

In the case of the seepage face at the bottom of a rectangular hillslope layout, $(\partial h/\partial x) = 0$ and $(\partial Q_s/\partial x) = 0$ accordingly, except for the downslope boundary. Therefore, over a seepage face of length $x_{sf} = n\Delta x$ (where $n \geq 1$), water seeps out only at the most downhill grid ($n = 1$). This is an artifact of the Dupuit assumption. Because over the seepage face the evapotranspiration occurs at its potential rate, the seepage outflow, averaged over the entire hillslope, amounts to

$$q_{sf} = \frac{Q_s(x_{sf}) - Q_s(0) - E_p n\Delta x}{x_L} \tag{24}$$

Case studies for simple hillslopes

Hillslope hydrological behaviour arises because of the complex interaction of many processes. In the remainder of this paper, application of the model to a simple reference case is used to examine the saturated-unsaturated zone interactions that yield distinct hydrological zones across the hillslope. For an analysis of the impact of various climate, soil and geomorphologic properties, the reader is referred to sensitivity studies in Salvucci and Entekhabi (1995) and Kim (1995).

SPECIFICATION OF CLIMATE, SOIL, GEOMORPHOLOGY AND VEGETATION PROPERTIES

Simulation of the hillslope hydrological behaviour using the proposed model requires specification of the initial and meteorological boundary conditions, the soil hydraulic parameters, the geomorphological layout and the vegetation characteristics. The initial conditions were chosen arbitrarily and the model was integrated for one year prior to the collection of the simulation diagnostics.

Climate forcing and soil hydraulic parameters

The intermittent atmospheric forcing is modelled as a Poisson arrival process of rectangular rainfall pulses interspersed with periods of constant potential evapotranspiration intensity (Eagleson, 1978b). A climate is specified entirely by the mean rainfall intensity, $\mu[\underline{i_r}]$, mean rainfall duration $\mu[\underline{t_d}]$, and mean interstorm duration $\mu[\underline{t_b}]$. The semi-humid parameters listed in Table 1 are defined by Salvucci and Entekhabi (1995) to represent an intermediate case of soil- versus climate-limits on hydrological fluxes.

For the soil hydraulic properties (4)–(6), the parameters of the loam soil, reported by Kim and Stricker (1996), are specified in Table 2.

Table 1. Parameters of the Poisson rectangular pulses model for rainfall and potential evapotranspiration for the arid, semi-humid and humid climate according to Salvucci and Entekhabi (1995).

Parameter	Semi-Humid
$\mu[\underline{i_r}]$ [mm d^{-1}]	50.7
$\mu[\underline{t_d}]$ [d]	0.25
$\mu[\underline{t_b}]$ [d]	3.44
E_p [mm d^{-1}]	3.3
Derived Statistics	
Mean Precipitation $\overline{P}$ [mm d^{-1}]	3.3
Mean Potential Evaporation $\overline{E_p}$ [mm d^{-1}]	3.1

Table 2. Van Genuchten (1980) parameters for the loam soil.

a_g^{ref} [m]	k_s^{ref} [m d^{-1}]	n_1	l	θ_s	θ_r
1.03	0.043	3.1	1.6	0.35	0.05

GEOMORPHOLOGICAL PARAMETERS AND GEOLOGIC CONTROLS

For simplicity and to compare the time-mean of the transient results with the equivalent-steady results of Salvucci and Entekhabi (1995), the analysis in this paper uses a simple hillslope (Fig. 1). It consists of a rectangle of soil on top of impermeable bedrock. The soil depth z_s is constant over the entire domain, as is the slope angle ϕ. The hillslope is supposed to form half of a symmetrical valley, such that the boundary at $x = 0$ can be taken as a no-flow boundary.

Note that for the rectangular hillslope layout and the Dupuit assumption in (9), seepage flow can occur only at the most downhill grid. The average seepage flow out of the hillslope is then given by (24). In reality, the flow is two-dimensional, the groundwater flow lines bend towards the surface and seepage is not restricted to the most downhill grid only.

Vegetation parameters

Root extraction in (7) and (8) is completely defined by the depth of the rootzone ($z_s - z_r$) and the values of θ_c and θ_w. The vegetation fully covers the soil surface across the hillslope. Bare soil evaporation is not treated explicitly; it is assumed that transpiration dominates the total evapotranspiration. The value of ($z_s - z_r$) used in this study is 0.2 meters. The values of θ_c and θ_w are given by (4) evaluated at ψ values of −5 m and −160 m respectively (Feddes, 1978). This implies that the amount of water available for transpiration depends on the soil hydraulic properties.

Numerical implementation

The horizontal node spacing $\Delta x = 1$ m is used for all cases. The vertical node spacing is taken as $\Delta z = 0.1$ m. The time step $\Delta t = 6$ min was chosen to prevent significant mass balance errors. The results presented here reflect time integrations over ten years, excluding a one year spin-up period to eliminate the effect of the arbitrarily chosen initial conditions. The storage change over this period is very small compared to the other terms in the water budget and is therefore neglected. Additional cases are reported by Kim (1995).

Results and discussion

The time-means of the dynamic hillslope hydrological response to intermittent storm and interstorm periods are

estimated. Figure 3 shows three graphs that summarize most of the hydrological phenomena acting on the hillslope defined in the Reference Case. The top panel shows the average position of the water table over the integration period of ten years. The second panel illustrates the magnitude of average evapotranspiration, recharge and surface runoff fluxes, normalized by the average rainfall. The third panel shows the lateral saturated and unsaturated flow. Going from the divide in the downhill direction to the valley, three regions can be distinguished.

In the uphill region ($\pm$ 30 m $\leq x \leq$ 75 m), the water table resides at relatively great depth, which prevents significant capillary rise and causes large storage capacity in the unsaturated zone. As a result, evapotranspiration and surface runoff fluxes are relatively small, resulting in a net recharge flux to the saturated zone (see Fig. 3a). This recharge causes the groundwater flow to increase downhill which in turn forces the water table to rise relative to the bedrock. Note that the mean evapotranspiration as a fraction of the mean rainfall $\bar{P}$ is 0.70, equivalent to a fraction of the mean potential evapotranspiration $\bar{E}_p$ of 0.75. On average, this points to considerable soil control on evapotranspiration (as opposed to available energy limitation) over this region.

The midslope region ($\pm$ 15 m $\leq x \leq$ 30 m), is characterized by a groundwater table being nearly parallel to the surface ($\partial h/\partial x \approx 0$). By virtue of (9), the average groundwater flow is relatively constant (Fig. 3c) and the average recharge in this zone is close to zero accordingly (see Fig. 3b). Although significant transient negative and positive recharge fluxes do occur, rainfall is partitioned mainly over evapotranspiration and surface runoff. Consistent with hydrogeological literature, this zone is called midline hereafter.

Near the valley (0 m $< x <$ $\pm$ 15 m), the water table approaches the surface because of the no-flow boundary condition at $x = 0$. The small storage capacity causes large surface runoff fluxes while large evapotranspiration fluxes during interstorm periods can be maintained because of capillary rise (negative recharge or discharge) from the phreatic surface (Fig. 3b). The amount of groundwater discharge through the seepage face is small (<1% of annual precipitation). The infiltration excess runoff mechanism is of little significance (also <1% of annual precipitation) for this combination of climate and soil hydraulic properties and virtually all surface runoff results from rain falling on saturated areas (20% of the annual rainfall). The numerical model exhibited about 4% error in total mass balance for the hillslope over the period of integration.

Qualitatively, this three zone structure is similar to the field observations of Toth (1966) and to that produced and analyzed using the statistical-dynamical model of Salvucci and Entekhabi (1995).

Finally, Fig. 3(c) shows the small amount of total mean unsaturated lateral flow $\overline{Q_u} = \int_h^{z_s} \overline{q_x}(z)dz$ relative to saturated lateral flow. Except for a small uphill region, where saturated flow is small, unsaturated lateral transport is nearly two orders of magnitude smaller than that in the saturated zone. Downhill, lateral transport in the unsaturated zone decreases because the phreatic surface becomes closer to the soil surface. Kim (1995) reports similar tests for hillslopes with varying soil types, geomorphologic and climate parameters, and soil anisotropy. The results generally confirm that the downslope spatial distributions of surface soil moisture and surface hydrological fluxes are clearly dominated by the two-way coupling of the saturated and unsaturated zones and by the groundwater lateral redistribution on hillslopes.

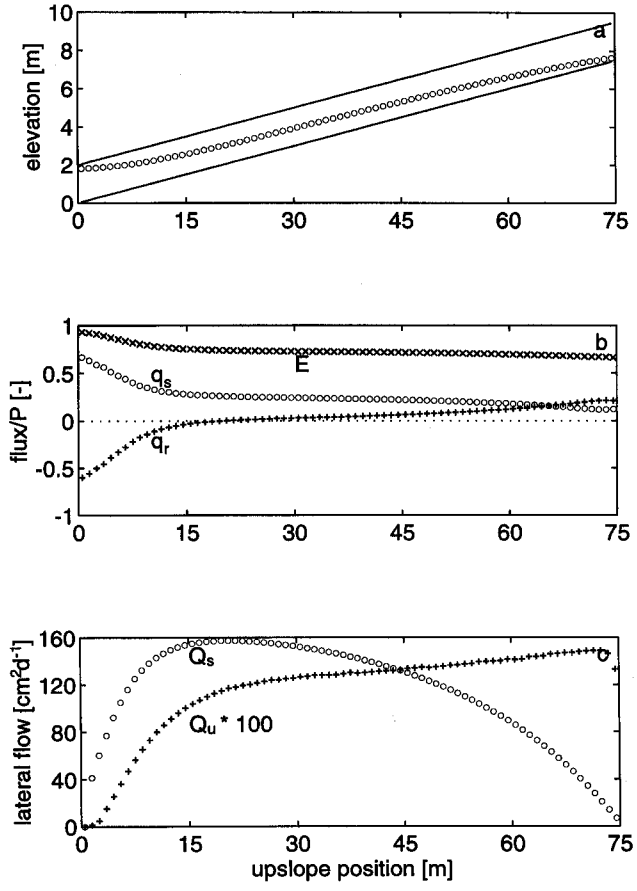

Fig. 3. *Ten year average results of the Reference Case: (a) Height of the phreatic surface h above the bedrock , (b) time average evapotranspiration $\bar{E}$, recharge $\overline{q_r}$, and total surface runoff $\overline{q_s}$ (= $\overline{q_{ie}}$ + $\overline{q_{se}}$) fluxes normalized by rainfall, and (c) magnitude of the mean lateral saturated flux Q_s and the mean lateral unsaturated flux Q_u.*

Mechanisms inducing midline region Equation (10) describes the dynamic behaviour of the phreatic surface and is taken as a starting point for the discussion. Firstly, the arguments put forth by Salvucci and Entekhabi (1995), describing the maintenance of the midline under equivalent steady conditions are reviewed. Next, the effects and impacts of transients are explored.

Equivalent-steady conditions Following Salvucci and Entekhabi (1995), consider the situation $\partial h/\partial t = 0$. From (10) it follows that the recharge is then equal to the divergence of the groundwater flow, i.e. $q_r = dQ_s/dx$. Where the water table is deep, the near-surface soil tends to be drier which restricts evapotranspiration, enhances infiltration, and thus promotes recharge. Where the water table is close to the surface, the near-surface soil stays moist because evapotranspiration losses are replenished by capillary rise from the water table. The moist soil also reduces net infiltration and promotes runoff with the water table often reaching the surface following storms. The net result is, that in the long-term mean, the groundwater discharges to the unsaturated zone. The functional relationship between the recharge and the depth to the phreatic surface, $q_r(z_s - h)$, depends on the soil hydraulic properties and the climatic conditions. Let h^* be defined by $q_r(z_s - h^*) = 0$. For the Reference Case in Fig. 3(a), $z_s - h^* \approx 100$ cm.

To see how the relation, $q_r(z_s - h)$, affects the water table structure, note that on a hillslope with a uniform soil, a situation where $dh/dx \leq 0$ would imply that the depth of the saturated zone increases uphill and that recharge would occur downhill and discharge uphill, which is physically impossible. Hence, the depth of the saturated zone becomes smaller uphill and $dh/dx > 0$ everywhere. Since over the midline region the phreatic surface runs parallel to the bedrock, i.e. $dh/dx = 0$, it then follows from (9) that

$$Q_s = k_s h \sin\phi \tag{25}$$

$$q_r = \frac{dQ_s}{dx} = k_s \frac{dh}{dx} \sin\phi = 0 \tag{26}$$

Thus, over the midline the saturated lateral water transport equals $Q_s = k_s h^* \sin\phi$ which is limited by the value h^*. Because of the no-flow condition at the divide x_L, the groundwater flow through the midline region is equal to the cumulative recharge uphill from position x^* where $h = h^*$:

$$k_s h^* \sin\phi = \int_{x^*}^{x_L} q_r(x)dx \tag{27}$$

The midline region thus acts as a restriction to the strength and the extent of the recharge zone through h^*, which depends on soil and climate parameters only (Salvucci and Entekhabi, 1995). At the downhill boundary, $x = 0$ and water can leave the hillslope only through a seepage face where the phreatic surface reaches the land surface. The extent of the midline region is thus restricted by the downhill boundary. When the lateral transport capacity is large or when the hillslope is short, the uphill recharge will be restricted directly by the downhill boundary and the midline collapses to a point where $h = h^*$ but $dh/dx < 0$. In geohydrological literature this point is referred to as hinge. Note that on longer hillslopes the recharge and discharge area remain unchanged while the midline makes up for the difference. In summary, for steady state conditions, the midline establishes a teleconnection between the recharge and the discharge zone; water lost as recharge uphill reappears in the water budget of the discharge zone, while leaving the budget of the midline unaffected.

Transient effects For transient conditions, the situation becomes slightly more complex. Using perturbation techniques, the groundwater flow is divided into one part that is explained by the mean condition of the phreatic surface (shown in Fig. 3a) and another part that is caused by transient deviations from the mean state. At any time and position, the depth of the saturated zone can be written in time-perturbation as:

$$h = \bar{h} + h' \qquad \bar{h}' = 0 \tag{28}$$

where the overline indicates the time average and the prime a transient deviation from the average. Insertion of (28) into (9) and subsequently taking the time average yields

$$\bar{Q}_s = k_s \bar{h} \cos\phi \left(\frac{\partial \bar{h}}{\partial x} + \tan\phi \right) + k_s \overline{h' \frac{\partial h'}{\partial x}} \cos\phi \tag{29}$$

The first term on the right hand side of (29) represents the lateral transport explained by the mean state (the equivalent steady representation), whereas the second term indicates the groundwater flow due to transient deviations from the mean state. The second term can be rewritten as

$$\begin{aligned} k_s \overline{h' \frac{\partial h'}{\partial x}} \cos\phi &= \tfrac{1}{2} k_s \frac{\overline{\partial h'^2}}{\partial x} \cos\phi \\ &= \tfrac{1}{2} k_s \frac{\partial \sigma^2[h]}{\partial x} \cos\phi \end{aligned} \tag{30}$$

where $\sigma^2[h]$ is the temporal variance of the water table position. Flow not accounted for in the equivalent steady analysis is thus proportional to the gradient of water table variance along the hillslope. Conceptually, the sources of water table variability can be separated into local effects such as water transfers with the unsaturated zone (e.g. infiltration fronts reaching the water table), and non-local effects related to the need to drain the net recharge uphill of a given point along the water table. Considering local effects, note that as one moves away from the channel the water table tends to reside deeper, yielding a larger unsaturated zone storage capacity and a longer time period for infiltration (and exfiltration) fronts to reach the water table. This leads to an attenuation of water table variability with increased water table depth from the surface (Salvucci and Entekhabi, 1994). For cases where the water table resides deeper as one moves uphill (e.g. near the divide/recharge zone, Fig. 3a), the water table variance will thus decrease (negative gradient) and there will be *less*

downhill flow than implied by the mean terms in (28). Essentially this represents a statistical analysis of groundwater ridging, in which the seepage face (or raised water table position) moves uphill due to more rapid response of the water table downhill.

The situation, however, is more complex near the channel. Near the channel, the ground surface acts as an upper limit to the magnitude of water table perturbations. Therefore, near the channel the water table variance tends to increase with distance uphill (a positive gradient), because there is more room for perturbations. This effect causes an increase in saturated lateral flow relative to the temporal mean analysis. Over the midline, where the water table depth is on average spatially constant, the variance due to local interaction with the vadose zone will also be nearly constant.

The other source of variation, i.e. variations in water table elevation brought about in response to integrated uphill recharge, is also tractable. Because the source of the perturbations is roughly proportional to the contributing recharge area and because the recharge itself is more uniform where the vadose zone is deeper, this source of variance will decrease uphill.

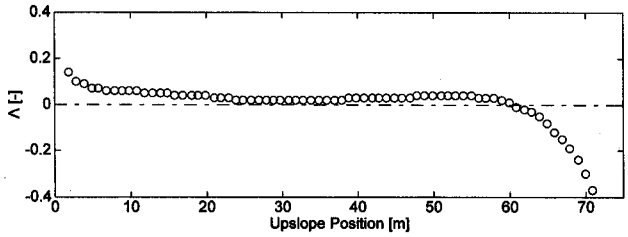

Fig. 4. *Magnitude of the non-dimensional term Λ which measures the degree of departure between time mean and equivalent-steady lateral saturated groundwater flow.*

Figure 4 illustrates the spatial pattern and relative importance of the perturbation flow term, plotted as a fraction of the mean lateral groundwater flow:

$$\Lambda = \frac{k_s \frac{\partial \sigma^2[h]}{\partial x} \cos\phi}{Q_s} \qquad (31)$$

As discussed above, the perturbations act to increase the lateral flow near the channel, are of minimal importance along the midline, and act to decrease flow near the divide. The net effect of this term is to make the three zone division derived through the equivalent steady state analysis of Salvucci and Entekhabi (1995) somewhat *less* distinct: the steady analysis depends on a strong lateral flow near the divide to drain the recharge zone, a divergence free midline, and weakened lateral flow near the channel due to evaporative losses. A true midline, in fact, will occur only where the water table variance is spatially exactly constant.

Overall, the variance term is not dominant in the case reported here (and in the other cases described in Kim(1995)). The conceptually simpler and more tractable equivalent steady-state framework may thus be applied to the analysis of long term mean surface water ground water interaction without seriously impacting predictive ability or understanding of these complex systems. The transient analysis does, however, aid in the interpretation of how pressure waves in the saturated zone act to destroy the organization of the hillslope into three regions which the saturated-unsaturated zone coupling, through the dependence of mean recharge on depth to water table, seeks to maintain.

Conclusions

A mixed analytical-numerical model of hillslope hydrological processes is presented. The model is applied to explore the role of transient effects in establishing the coupling between saturated and unsaturated zones on hillslopes. The model is computationally efficient for integration over very long periods (ten years) with a high lateral resolution.

The investigation results indicate that over hillslopes the magnitude of unsaturated lateral flow is very small compared to the lateral groundwater flow. The downslope spatial distributions of surface soil moisture and surface hydrological fluxes are clearly dominated by the two-way coupling of the saturated and unsaturated zones and by the groundwater lateral redistribution on hillslopes.

Hydrological flux over hillslopes is divided into three regions with distinct characteristics. A recharge and a discharge zone are connected by a midline region, as found by Toth (1966) in the Canadian prairies and by Salvucci and Entekhabi (1995) in a statistical-dynamical model. This division induces an internal hillslope teleconnection between the uphill recharge and the downhill discharge zones.

Spatial head covariance terms are derived; these distinguish the time-averaged phreatic surface from the equivalent-steady surface derived by Salvucci and Entekhabi (1995). The covariance terms are shown to smooth, but not significantly alter, the three-zone structure determined by the equivalent-steady analysis.

Acknowledgments

The comments of Reinder Feddes and Han Stricker significantly improved the presentation. The first author acknowledges the financial contribution of the Netherlands Organization for Scientific research (NWO). This study was also supported by NASA grant NAS 5-31721. John MacFarlane is also thanked for his assistance with some figures.

References

Beven, K. J. and Kirkby, M. J., 1979. A physically-based variable contributing area model of basin hydrology, *Hydrol. Sci. Bull.*, **24**, 43–69.

Dawes, W. R., Zhang, L., Hatton, T. J., Reece, P. H., Beale, G. T. H. and Packer, I., 1997. Evaluation of a distributed parameter ecohydrological model (TOPOG_IRM) on a small cropping rotation catchment, *J. Hydrol.*, **191**, 67–89.

Eagleson, P. S. 1978a. Climate, soil and vegetation 1. Introduction to water balance dynamics. *Wat. Resour. Res.*, 14, 705–712.

Eagleson, P. S., 1978b. Climate, soil and vegetation 2. The distribution of annual precipitation derived from observed storm sequences. *Wat. Resour. Res.*, **14**, 713–721.

Feddes, R. A., Kowalik, P. J., and Zaradny, H., 1978. *Simulation Model of the Water Balance of a Cropped Soil.* Simulation Monograph. PUDOC, Wageningen, The Netherlands. pp. 189.

Freeze, R. A., 1971. Three-dimensional., transient, saturated-unsaturated flow in a groundwater basin. *Wat. Resour. Res.*, 7, 347–366.

Freeze. R. A. and Witherspoon, P. A., 1968. Theoretical analysis of regional groundwater flow, 3. Quantitative interpretations. *Wat. Resour. Res.*, 4, 581–590.

Kim, C. P., 1995. *The Water Budget of Heterogeneous Areas; Impact of Soil and Rainfall Variability.* Ph.D. thesis, Wageningen Agricultural University, Netherlands. pp, 183.

Kim, C. P. and Stricker, J. N. M., (1996). Influence of spatially variable soil hydraulic properties and rainfall intensity on the water budget. *Wat. Resour. Res.*, **32**, 1699–1712.

Kutilek, M., and Nielsen, D., 1994. *Soil Hydrology*, Catena Verlag, Destedt, 369p.

Milly, P. C. D. and Eagleson, P. S., 1987. Effects of spatial variability on annual average water balance, *Wat. Resour. Res.*, **23**, 2135–2142.

Paniconi C. and Wood, E. F., (1993): A detailed model for simulation of catchment scale subsurface hydrological processes. *Wat. Resour. Res.*, **29**, 1601–1620.

Peck, A. J., Luxmoore, R. J. and Stolzy, J. L., 1977. Effects of spatial variability of soil hydraulic properties in water budget modeling, *Wat. Resour. Res.*, 13, 348–354.

Salvucci, G. D. and Entekhabi, D., 1994. Equivalent steady soil moisture profile and time compression approximation in water balance modeling, *Wat. Resour. Res.*, **30**, 2737–2750.

Salvucci, G. D. and Entekhabi, D., 1995. Hillslope and climatic controls of hydrological fluxes, *Wat. Resour. Res.*, **31**, 1725–1739.

Sivapalan, M., Beven, K. J. and Wood, E. F., 1987. On hydrological similarity: 2. A scaled model of storm runoff production, *Wat. Resour. Res.*, **23**, 2266–2278.

Smith, R. E., Corradini, C., and Melone, F., 1993. Modeling infiltration for multistorm runoff events. *Wat. Resour. Res.*, **29**, 133–143.

Smith, R. E. and Hebbert, R. H. B., 1983. Mathematical simulation of interdependent surface and subsurface hydrological processes. *Wat. Resour. Res.*, **19**, 987–1001.

Toth, J., 1966. Mapping and interpretation of field phenomena for groundwater reconnaissance in a prairie environment, Alberta, Canada, *Bull. Int. Assoc. Sci. Hydrol.*, 11, 1–49.

Troch, P. A., De Troch, F. P. and Brutsaert, W., 1993. Effective water table depth to describe initial conditions prior to storm rainfall in humid regions, *Wat. Resour. Res.*, 29, 427–434.

Van Genuchten, M. T., 1980. A closed-form equation for predicting the hydraulic conductivity of unsaturated soil, *Soil Sci. Soc. Am. J.*, **44**, 892–898.

Zaidel, J. and Russo, D., 1993. Estimation of finite difference interblock conductivities for simulation of infiltration into initially dry soils. *Wat. Resour. Res.*, **29**, 2285–2295.